nature genetics

Mutations at a single codon in Mad homology 2 domain of SMAD4 cause Myhre syndrome

Carine Le Goff[1], Clémentine Mahaut[1], Avinash Abhyankar[2], Wilfried Le Goff[3], Valérie Serre[1], Alexandra Afenjar[4], Anne Destrée[5], Maja di Rocco[6], Delphine Héron[7], Sébastien Jacquemont[8], Sandrine Marlin[9], Marleen Simon[10], John Tolmie[11], Alain Verloes[12], Jean-Laurent Casanova[2,13], Arnold Munnich[1] & Valérie Cormier-Daire[1]

Myhre syndrome (MIM 139210) is a developmental disorder characterized by short stature, short hands and feet, facial dysmorphism, muscular hypertrophy, deafness and cognitive delay. Using exome sequencing of individuals with Myhre syndrome, we identified *SMAD4* as a candidate gene that contributes to this syndrome on the basis of its pivotal role in the bone morphogenetic pathway (BMP) and transforming growth factor (TGF)-β signaling. We identified three distinct heterozygous missense *SMAD4* mutations affecting the codon for Ile500 in 11 individuals with Myhre syndrome. All three mutations are located in the region of *SMAD4* encoding the Mad homology 2 (MH2) domain near the site of monoubiquitination at Lys519, and we found a defect in SMAD4 ubiquitination in fibroblasts from affected individuals. We also observed decreased expression of downstream TGF-β target genes, supporting the idea of impaired TGF-β–mediated transcriptional control in individuals with Myhre syndrome.

Myhre syndrome is a well-defined disorder characterized by pre- and postnatal short stature, brachydactyly, facial dysmorphism (short palpebral fissures, maxillary hypoplasia, prognathism and short philtrum), thick skin, generalized muscle hypertrophy and restricted joint mobility[1]. Deafness that is of mixed conductive and sensory types is consistently observed in older individuals with this syndrome. Other features include developmental delay with mental retardation and/or behavioral disturbance, cardiac defects, cryptorchidism and bone anomalies. Skeletal manifestations include thickened calvarium, cone-shaped epiphyses, shortened tubular bones, hypoplastic iliac wings, broad ribs and large vertebrae with short and large pedicles[2]. Myhre syndrome is differentially diagnosed as stiff skin syndrome (SSS)[3] and as acromelic dysplasia, including Weill-Marchesani syndrome (WMS)[4] and acromicric and geleophysic dysplasias, all of which are also characterized by short stature and brachydactyly[5]. Myhre syndrome is distinguished from these three other disorders[4,5] by different facial features, developmental delay, deafness and distinct skeletal features. Whereas *ADAMTS10* and *ADAMTSL2* mutations have been identified in the recessive forms of WMS and geleophysic dysplasia[6–8], *FBN1* mutations have been identified in SSS and acromicric dysplasia and in the dominant forms of WMS and geleophysic dysplasia[3,5,9].

All reported cases of Myhre syndrome are sporadic, and a few instances have been reported in which affected individuals had parents of advanced age at the time of birth, supporting the idea that the syndrome results from the *de novo* acquisition of dominant mutations[2].

We collected DNA samples from 11 individuals with Myhre syndrome (cases), all of whom fulfilled the diagnostic criteria for the syndrome (**Fig. 1** and **Supplementary Table 1**). To identify the causal gene for this disease, we performed exome sequencing in 2 out of the 11 probands. We first focused on the identification of nonsynonymous variants, splice acceptor and donor site mutations and insertions and deletions (indels) affecting coding regions, anticipating that synonymous variants were far less likely to be pathogenic. We regarded variants as previously unidentified if they were absent from control populations and from in house exome data and all publically available data sets, including those of dbSNP129 and the 1000 Genomes Project.

Assuming a model in which mutations have dominant effects, we identified 19 candidate genes through exome analysis (**Supplementary Table 2**). Taking into account our previous findings of enhanced TGF-β signaling in geleophysic and acromycric dysplasias, we selected *SMAD4* (mothers-against-DPP homolog 4; NM _005359) as the best

[1]Département de Génétique, Unité INSERM U781, Université Paris Descartes, Sorbonne Paris Cité, Hôpital Necker Enfants Malades, Paris, France. [2]St. Giles Laboratory of Human Genetics of Infectious Diseases, Rockefeller Branch, The Rockefeller University, New York, New York, USA. [3]INSERM, Unité Mixte de Recherche (UMR) S939, Dyslipidemia, Inflammation and Atherosclerosis in Metabolic Diseases, University of Pierre and Marie Curie (UPMC)–Université Paris VI, Paris, France. [4]Service de Neuropédiatrie, Centre de Référence Anomalies du Développement, Hôpital Armand Trousseau, Paris, France. [5]Institut de Génétique Humaine, Insitute de Pathologie et de Génétique (IPG), Charleroi, Belgium. [6]Unit of Rare Diseases, Department of Pediatrics, Gaslini Institute, Genoa, Italy. [7]Unité de Génetique Clinique, Hôpital La Pité Salpétrière, Paris, France. [8]Service de Génétique Médicale, Centre Hospitalier Universitaire Vaudois (CHUV), Lausanne, Switzerland. [9]Unité de Génétique Clinique, Hôpital Armand Trousseau, Paris, France. [10]Department of Clinical Genetics, Erasmus MC University Medical Center, Rotterdam, The Netherlands. [11]Department of Medical Genetics, Ferguson Smith Centre, Yorkhill Hospital, Glasgow, UK. [12]Département de Génétique, INSERM U676, Hôpital Robert Debré, Paris, France. [13]Laboratory of Human Genetics of Infectious Diseases, University Paris Descartes and INSERM U980, Necker Medical School, Paris, France. Correspondence should be addressed to V.C.-D. (valerie.cormier-daire@inserm.fr).

Received 4 August; accepted 31 October; published online 11 December 2011; doi:10.1038/ng.1016

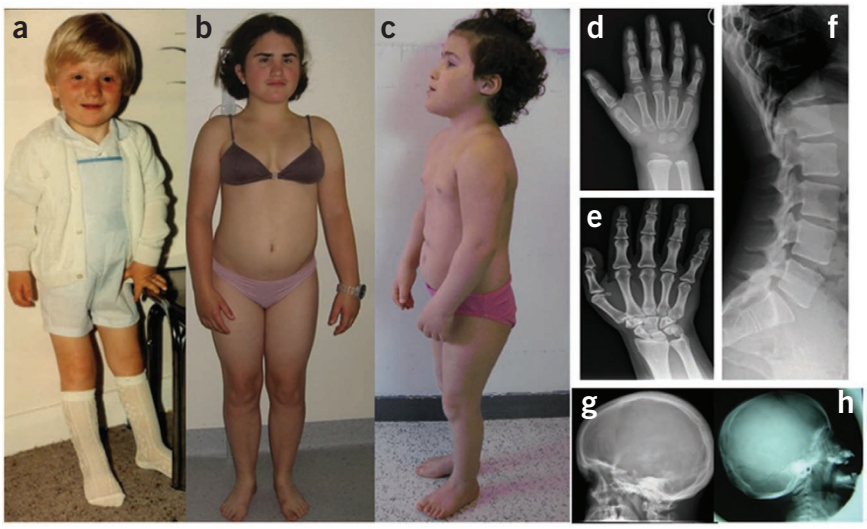

Figure 1 Clinical and radiological manifestations of individuals with Myhre syndrome. (**a**–**c**) Photographs of affected individuals at ages 4 years (case 8) (**a**), 16 years (case 5) (**b**) and 8 years (case 1) (**c**). Note the short palpebral fissures, maxillary hypoplasia, prognathism, muscular build and short extremities. (**d**,**e**) Hand X rays are shown for affected individuals at ages 4 years (**d**) and 14 years (**e**). Note the generalized brachydactyly and delayed carpal ossification at age 4 years. (**f**) Spine X ray of a case at age 14 years. Note the large vertebrae with short and large pedicles. (**g**,**h**) Skull X rays of cases at age 10 years (**g**) and age 16 years (**h**). Note the thickened calvarium. Informed consent was obtained from all individuals or the legal guardians of minors.

candidate causal gene for Myhre syndrome on the basis of its involvement in the TGF-β and BMP signaling pathways. Exome analysis detected the same heterozygous missense mutation (c.1498A>G; encoding p. Ile500Thr) in *SMAD4* in both Myhre syndrome cases that were sequenced. The presence of this mutation was confirmed by Sanger sequencing.

The 11 coding exons of *SMAD4* are translated into a 552-residue protein composed of a Mad homology 1 (MH1) domain that is involved in DNA binding, a linker and an MH2 domain involved in transcriptional activation[10]. Direct sequence analysis of the coding regions in nine additional Myhre syndrome cases led to the identification of three missense mutations in the region of *SMAD4* coding for the MH2 domain, all affecting an isoleucine residue at position 500 (p.Ile500Thr, p.Ile500Val and p.Ile500Met) (**Table 1** and **Supplementary Fig. 1**). These alterations were considered to be pathogenic by the PolyPhen database, as Ile500 is highly conserved across species. The alterations were absent from 200 ancestry-matched controls and were not observed in the parents of individuals with Myhre syndrome, confirming that these mutations are acquired in a *de novo* manner.

SMAD4 encodes a protein belonging to the eight-member family of SMADs, which is divided into three functional classes: the receptor-regulated SMADs (R-SMADs: SMAD1, SMAD2, SMAD3, SMAD5 and SMAD8), the co-mediator SMAD (SMAD4) and the inhibitory SMADs (SMAD6 and SMAD7). SMAD2 and SMAD3 respond to TGF-β and activin, and SMAD1, SMAD5 and SMAD8 function in BMP signaling pathways. After being activated, receptor-regulated SMADs form heterodimers with SMAD4 and translocate into the nucleus to induce or repress the expression of TGF-β and BMP target genes[11].

Table 1 ***SMAD4*** **mutations identified in Myhre syndrome cases**

Family	Nucleotide change	Amino acid change
1	c.1499T>C	p.Ile500Thr
2	c.1499T>C	p.Ile500Thr
3	c.1498A>G	p.Ile500Val
4	c.1499T>C	p.Ile500Thr
5	c.1498A>G	p.Ile500Val
6	c.1498A>G	p.Ile500Val
7	c.1499T>C	p.Ile500Thr
8	c.1500A>G	p.Ile500Met
9	c.1498A>G	p.Ile500Val
10	c.1498A>G	p.Ile500Val
11	c.1499T>C	p.Ile500Thr

To determine the functional impact of *SMAD4* mutations, we assessed the level of SMAD4 in cultured skin fibroblasts from cases by protein blot analysis and found enhanced levels of SMAD4 in two Myhre syndrome cases (cases 1 and 4), contrasting with a weak endogenous level of SMAD4 in age- and passage-matched control skin fibroblasts (**Fig. 2a**).

We performed *in silico* analysis to further study the effect of the mutations. None of the mutations seemed to disrupt the intricate network of hydrogen bonding at the protein interface; however, a local destabilization in the protein-protein interface cannot be excluded. Moreover, as SMAD4 is monoubiquitinated at Lys519, which is located close to Ile500 in the three-dimensional structure of SMAD4, an impairment of the ubiquitination process could also explain our finding of elevated protein levels of mutant SMAD4 (**Supplementary Fig. 2**).

To analyze the extent to which SMAD4 is ubiquitinated, we performed protein blot analysis of immunoprecipitated SMAD4 from fibroblast lysates of case 1 and two age- and passage-matched controls. We found decreased ubiquitination of SMAD4 in cells from the Myhre syndrome case, supporting the idea that there is increased stabilization of the mutant SMAD4 relative to the wild-type protein (**Fig. 2b**).

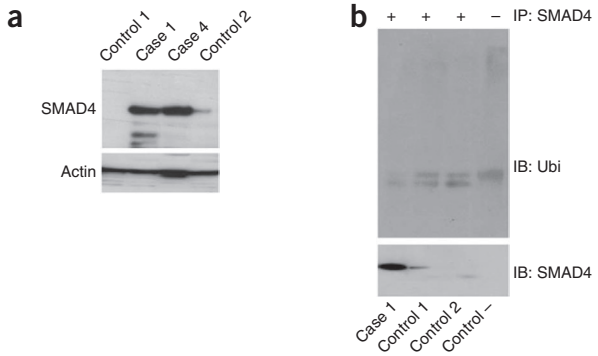

Figure 2 Functional consequences of *SMAD4* mutations in fibroblasts from individuals with Myhre syndrome. (**a**) Characterization of wild-type and mutant SMAD4 protein expression. Increased levels of SMAD4 were seen for mutant SMAD4 (from cases 1 and 4) compared to wild-type SMAD4. (**b**) Ubiquitination of wild-type and mutant SMAD4. SMAD4 was immunoprecipitated from cell lysates, and protein blots were performed with an antibody that recognizes ubiquitinated proteins. Mutated SMAD4 (in case 1) was ubiquitinated to a lesser extent than wild-type SMAD4 proteins.

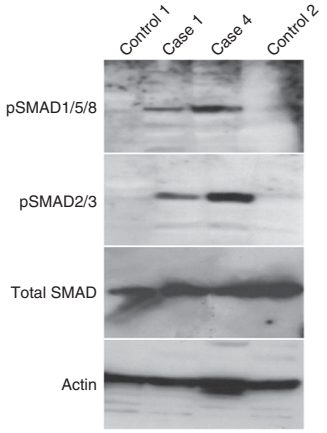

Figure 3 Levels of phosphorylated SMAD proteins in skin fibroblasts from individuals with Myhre syndrome and age- and passage-matched controls. Enhanced levels of phosphorylation of SMAD2/3 and of SMAD/5/8 were seen in cells from subjects with Myhre syndrome (cases 1 and 4) compared to controls. The levels of phosphorylated SMADs were normalized to total SMAD protein.

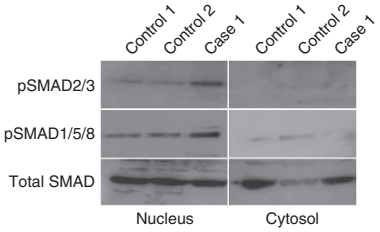

Figure 4 Cellular localization of phosphorylated SMAD proteins. Phosphorylated SMAD2/3 and phosphorylated SMAD1/5/8 localized to the nucleus in fibroblasts cultured from case 1.

Because SMAD4 has a pivotal role in TGF-β and BMP signaling, we analyzed the level of phosphorylation of SMAD2/3 and of SMAD1/5/8 in fibroblast lysates from cases 1 and 4 (**Fig. 3**). We found an 8-fold increase in the levels of phosphorylated SMAD2/3 and an 11-fold increase in the amount of phosphorylated SMAD1/5/8 in the cell lysates of cases relative to controls.

We then studied the localization of the phosphorylated SMAD proteins by protein blotting and found an enhanced presence of phosphorylated SMADs in the nucleus of fibroblasts from case 1 compared to controls, which coincided with a weak signal in the cytoplasm of the fibroblasts from the affected individual, supporting the idea that active SMAD complexes are being translocated into the nucleus in these cells (**Fig. 4**).

We finally measured the effect of these mutant complexes on TFG-β– and BMP-driven transcription. Using quantitative RT-PCR, we found decreased mRNA levels of downstream TGF-β targets, namely *CTGF* (connective tissue growth factor), *Col1A1* (collagen type 1, α1) and *SERPINE1* (also known as *PAI-1*, plasminogen activator inhibitor 1), and variable effects on BMP targets, with decreased expression of *ID3* (inhibitor of DNA binding) and increased expression of *SMAD6* (**Fig. 5**).

Here we report the identification of heterozygous *SMAD4* mutations in 11 cases presenting with the characteristic features of Myhre syndrome. We observed *de novo* mutations in all cases examined, thus providing evidence for a dominant mode of inheritance for Myhre syndrome. Moreover, we observed heart, urogenital, intestinal, velopharyngeal and eye anomalies in the cases in this study, a finding that expands the phenotypic spectrum of this disorder and provides evidence for a key role of SMAD4 in development.

Of note, mice with homozygous loss of *Smad4* die before embryonic day 7.5 (E7.5), and mutant embryos are smaller than wild-type mice at the same gestational stage[12]. Conditional knockout of *Smad4* in chondrocytes results in dwarfism, which is accompanied by severely disorganized growth plates and decreased activation of Indian hedgehog–parathyroid hormone–related protein (Ihh-PTHrP) signaling, supporting the view that Smad4-mediated TGF-β signaling is required to insure the normal organization of chondrocytes in the growth plate[13]. Mice with conditional *Smad4* deletion in chondrocytes are also characterized by a smaller cochlear volume[14], and anomalies of the osseous spiral lamina and basilar membrane lead to severe sensorineural hearing loss, as also observed in persons with Myhre syndrome, supporting a role for Smad4 in inner ear development and normal auditory function. Finally, the targeted ablation of *Smad4* in osteoblasts revealed that Smad4 is also required for maintaining normal postnatal bone homeostasis in mice[15]. This function of Smad4 may explain the thick calvarium and facial features (including prognatism and maxillary hypoplasia) observed in persons with Myhre syndrome.

This is the first report linking a unique amino acid change involving Ile500 of SMAD4 within the MH2 domain with a developmental disorder. Until now, SMAD4 has been considered to be a tumor suppressor. Loss-of-function *SMAD4* mutations have been reported in juvenile polyposis syndrome that is characterized by the presence of juvenile polyps in the gastrointestinal tract and increased colorectal cancer risk[16]. Inactivation of SMAD4 has also been demonstrated in cases of pancreatic and colorectal carcinoma[17,18]. Tumors lacking functional SMAD4 tend to be more invasive and angiogenic and are consequently more likely to form metastatic lesions[19]. It is known that the disruption of TGF-β signaling contributes to the development of human malignancies[20], and instability of the SMAD4 protein may contribute to a loss in cellular responsiveness to TGF-β signaling in tumors[21].

In contrast with these previously observed activities of SMAD4 in cancer, decreased levels of SMAD4 ubiquitination and increased levels of SMAD4 protein suggest a stabilization of SMAD4 in Myhre syndrome. Functional SMAD4 is required for canonical signal transduction through its oligomerization with phosphorylated SMAD2/3 in the TGF-β pathway and with phosphorylated SMAD1/5/8 in the BMP pathway. The nuclear localization of complexes containing stabilized

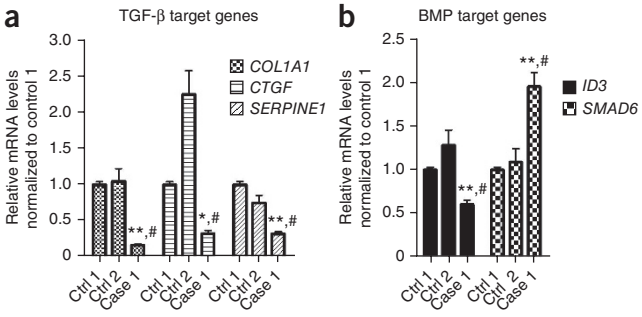

Figure 5 Expression analysis of TGF-β– and BMP-driven target genes in fibroblasts from control and case subjects. (**a**,**b**) Quantification of the mRNA levels of *COL1A1*, *CTGF* and *SERPINE1* (TGF-β signaling pathway) (**a**) and *ID3* and *SMAD6* (BMP signaling pathway) (**b**) was performed by quantitative RT-PCR in fibroblasts from controls (controls 1 and 2) and a case (case 1). mRNA levels were normalized to the expression of housekeeping genes (*HSP90AA1* and *NONO*) and to 18S rRNA levels. Values are expressed as mean ± s.e.m. ($N = 6$; $^{\#}P < 0.01$ compared to control 2; $^{*}P < 0.05$, $^{**}P < 0.01$ compared to control 1.)

mutant SMAD4 that we observed in the fibroblasts of Myhre syndrome cases support the idea that mutant SMAD4 is capable of binding to and oligomerizing with pSMADs and can translocate to the nucleus.

Taking into account the involvement of the MH2 domain in transcriptional activation, our findings of the impaired expression of TGF-β–driven target genes further supports the idea that complexes containing mutant SMAD4 are defective in transcriptional regulation. Although enhanced levels of *SMAD6* demonstrate the integrity of the negative feedback loop of the TGF-β and BMP pathways, the mechanism of *SMAD6* upregulation is still not understood. Finally, because SMAD4 is not regulated by phosphorylation, ubiquitination might also have a role in the regulation of SMAD4 function.

Because fibroblasts were only available from two individuals with Myhre syndrome, the ability to make generalized conclusions based on this study is limited. Of note, however, the three mutations identified in the 11 cases all affected the same amino acid, Ile500, which lends support to the hypothesis that these alterations have identical functional consequences. Ongoing studies will further elucidate the context-dependent mechanisms and tissue-specific consequences of SMAD4-mediated TGF-β and BMP signaling and may inspire novel pharmacological strategies to target these complex pathways.

URLs. Picard, http://picard.sourceforge.net/; Swiss-Pdb Viewer 3.7, http://www.expasy.org/spdbv/.

METHODS

Methods and any associated references are available in the online version of the paper at http://www.nature.com/naturegenetics/.

Note: Supplementary information is available on the Nature Genetics website.

ACKNOWLEDGMENTS

We are grateful to the individuals with Myhre syndrome and their families for their participation in this study. We also thank the following physicians for the management of the affected individuals: D. Doummar, R. McGowan, P. Picco and M. Whiteford. This research was supported by the French National Research Agency (ANR; R09183KS to V.C.-D.).

AUTHOR CONTRIBUTIONS

C.L.G. designed the experiments, analyzed the exome sequencing data, performed protein blot analysis and wrote the manuscript. C.M. performed Sanger sequencing analysis. A. Abhyankar and J.-L.C. performed exome capture. W.L.G. performed quantitative RT-PCR analysis. V.S. performed three-dimensional structure analysis. A. Afenjar, A.D., M.d.R., D.H., S.J., S.M., M.S., J.T. and A.V. provided clinical data. A.M. wrote the manuscript. V.C.-D. provided clinical data, analyzed the exome sequencing data, oversaw all aspects of the research and wrote the manuscript.

COMPETING FINANCIAL INTERESTS

The authors declare no competing financial interests.

Published online at http://www.nature.com/naturegenetics/.
Reprints and permissions information is available online at http://www.nature.com/reprints/index.html.

1. Myhre, S.A., Ruvalcaba, H.A. & Graham, C.B. A new growth deficiency syndrome. *Clin. Genet.* **20**, 1–5 (1981).
2. Burglen, L. *et al.* Myhre syndrome: new reports, review, and differential diagnosis. *J. Med. Genet.* **40**, 546–551 (2003).
3. Loeys, B.L. *et al.* Mutations in fibrillin-1cause congenital scleroderma: stiff skin syndrome. *Sci. Transl. Med.* **2**, 23ra20 (2010).
4. Faivre, L. *et al.* Clinical homogeneity and genetic heterogeneity in Weill-Marchesani syndrome. *Am. J. Med. Genet.* **123**, 204–207 (2003).
5. Le Goff, C. *et al.* Mutations in the TGF-β binding-protein-like domain 5 of *FBN1* are responsible for acromicric and geleophysic dysplasias. *Am. J. Hum. Genet.* **89**, 7–14 (2011).
6. Dagoneau, N. *et al. ADAMTS10* mutations in autosomal recessive Weill-Marchesani syndrome. *Am. J. Hum. Genet.* **75**, 801–806 (2004).
7. Le Goff, C. *et al. ADAMTSL2* mutations in geleophysic dysplasia demonstrate a role for ADAMTS-like proteins in TGF-β bioavailability regulation. *Nat. Genet.* **40**, 1119–1123 (2008).
8. Allali, S. *et al.* Molecular screening of *ADAMTSL2* gene in 33 patients reveals the genetic heterogeneity of geleophysic dysplasia. *J. Med. Genet.* **48**, 417–421 (2011).
9. Faivre, L. *et al.* In-frame fibrillin-1 gene deletion in autosomal dominant Weill-Marchesani syndrome. *J. Med. Genet.* **40**, 34–36 (2003).
10. Ross, S. & Hill, C.S. How the Smads regulate transcription. *Int. J. Biochem. Cell Biol.* **40**, 383–408 (2008).
11. Shi, Y. & Massague, J. Mechanisms of TGF-β signaling from cell membrane to the nucleus. *Cell* **113**, 685–700 (2003).
12. Sirard, C. *et al.* The tumor suppressor gene *Smad4/Dpc4* is required for gastrulation and later anterior development of the mouse embryo. *Genes Dev.* **12**, 107–119 (1998).
13. Zhang, J. *et al.* Smad4 is required for the normal organization of the cartilage growth plate. *Dev. Biol.* **284**, 311–322 (2005).
14. Yang, S.M. *et al.* Chondrocyte- specific *Smad4* gene conditional knockout results in hearing loss and inner ear malformation in mice. *Dev. Dyn.* **238**, 1897–1908 (2009).
15. Tan, X. *et al.* Smad4 is required for maintaining normal murine postnatal bone homeostasis. *J. Cell Sci.* **120**, 2162–2170 (2007).
16. Howe, J.R. *et al.* Mutations in the *SMAD4/DPC4* gene in juvenile polyposis. *Science* **280**, 1086–1088 (1998).
17. Schutte, M. *et al. DPC4* gene in various tumor types. *Cancer Res.* **56**, 2527–2530 (1996).
18. Hahn, S.A. *DPC4*, a candidate tumor suppressor gene at human chromosome 18q21.1. *Science* **271**, 350–353 (1996).
19. Sunamura, M. *et al.* Gene therapy for pancreatic cancer based on genetic characterization of the disease. *J. Hepatobiliary Pancreat. Surg.* **9**, 32–38 (2002).
20. Kurokawa, M. *et al.* The oncoprotein Evi-1 repress TGF-β signaling by inhibiting Smad3. *Nature* **394**, 92–96 (1998).
21. Xu, J. & Attisano, L. Mutations in the tumor suppressors Smad2 and Smad4 inactivate transforming growth factor β signaling by targeting Smads to the ubiquitin-proteasome pathway. *Proc. Natl. Acad. Sci. USA* **97**, 4820–4825 (2000).

ONLINE METHODS

Subjects. A total of 11 individuals with Myhre syndrome were included in the study. They all fulfilled the following inclusion criteria: short stature, short hands, restricted joint limitation, thick skin, characteristic facial features, deafness and developmental delay (**Fig. 1** and **Supplementary Table 1**). Informed consent was obtained in accordance with the ethical standards of the Institutional Review Board (IRB) on Human Experimentation.

Exome sequencing. We collected blood samples from affected individuals and performed massively parallel sequencing. DNA (3 μg) was extracted from leukocyte cells from the cases and was sheared with a Covaris S2 Ultrasonicator. An adaptor-ligated library was prepared with the Paired-End Sample Prep kit V1 (Illumina). Exome capture was performed with the SureSelect Human All Exon kit (Agilent)[22]. Single-end sequencing was carried out on an Illumina Genome Analyzer II× that generated 72-bp reads. For sequence alignment, variant calling and annotation, the sequences were aligned to the human genome reference sequence (hg18 build) using the Burrows-Wheeler Aligner (BWA)[23]. Downstream processing was carried out with the Genome analysis toolkit (GATK)[24], SAMtools[25] and Picard Tools. Substitution calls were made with a GATK Unified Genotyper, and indel calls were made with a GATK IndelGenotyperV2. All calls with a read coverage ≤2× and a Phred-scaled SNP quality of ≤20 were removed from consideration. All variants were annotated using an annotation software system that was developed in house.

Mutation detection. We designed a series of 12 intronic primers to amplify the 11 coding exons of *SMAD4* (**Supplementary Table 3**). We purified the amplicons and sequenced them using the fluorescent dideoxy-terminator method on an automatic sequencer (ABI 3100; Applied Biosystems).

Protein blotting. For protein blot analysis of SMAD4 and phosphorylated SMADs, cell lysates were obtained from skin fibroblasts (from controls and cases 1 and 4). Antibodies recognizing actin (Invitrogen), phosphor-Smad2 (Ser465/467)/Smad3 (Ser423/425) (9510) and phosphor-Smad1 (Ser463/465)/Smad5 (Ser463/465)/Smad8 (Ser426/428) (9511) (both from Cell Signaling Technology) were used. The levels of phosphorylated SMADs were normalized to total SMAD protein (detected using clone C-17; sc-6030, Santa Cruz Biotechnology).

Three-dimensional structure of human SMAD4. Swiss-Pdb Viewer 3.7 (see URLs) was used to analyze the structural consequences of *SMAD4* mutations.

Ubiquitination assays. Fibroblasts from case 1 and control subjects were lysed in IP Lysis Buffer (87787; Pierce), and protein concentration was determined using the BCA Protein Assay (23227; Pierce) method. Protein from lysed cells (500 μg) was incubated with antibody recognizing SMAD4 (clone EP618Y; ab40759, Abcam) at 4 °C overnight, and the Catch and Release kit (Cell Signaling Technology) was used for immunoprecipitation. To detect ubiquitination of precipitated SMAD4, protein blot analysis was performed using antibody to ubiquitinated proteins (clone FK2; 04-263, Millipore). Normal rabbit serum was used in the immunoprecipitation step as a negative control.

Cellular localization of phosphorylated SMAD proteins. Fibroblasts from control subjects and case 1 were isolated and washed with PBS. We carried out cytoplasmic and nuclear protein extraction using reagent from the NE-PER kit (Pierce). Protein concentration was assessed with by using BCA Protein Assay. We then performed protein blot analysis with the antibodies described above.

RNA extraction, reverse-transcription and quantitative PCR. Monolayers of human fibroblasts isolated from skin biopsies of control subjects and case 1 were washed twice with cold PBS and total RNA was extracted using a NucleoSpin RNA II kit (Macherey-Nagel) according to the manufacturer's instructions. Reverse transcription of RNA and quantitative RT-PCR (LightCycler LC480; Roche) were performed as previously described (**Supplementary Table 4**)[26]. mRNA levels were normalized to the expression of housekeeping genes (*HSP90AA1* and *NONO*) and to the levels of human 18S rRNA. Data were expressed as a fold change in mRNA expression relative to values seen in cells from control subjects.

22. Byun, M. *et al.* Whole-exome sequencing-based discovery of STIM1 deficiency in a child with fatal classic Kaposi sarcoma. *J. Exp. Med.* **207**, 2307–2312 (2010).
23. Li, H. & Durbin, R. Fast and accurate short read alignment with Burrows-Wheeler transform. *Bioinformatics* **25**, 1754–1760 (2009).
24. McKenna, A. *et al.* The Genome Analysis Toolkit: a MapReduce framework for analyzing next-generation DNA sequencing data. *Genome Res.* **20**, 1297–1303 (2010).
25. Li, H. *et al.* The Sequence Alignment/Map format and SAMtools. *Bioinformatics* **25**, 2078–2079 (2009).
26. Larrede, S. *et al.* Stimulation of cholesterol efflux by LXR agonists in cholesterol-loaded human macrophages is ABCA1-dependent but ABCG1-independent. *Arterioscler. Thromb. Vasc. Biol.* **29**, 1930–1936 (2009).